Bulletin of the Seismological Society of America, Vol. 78, No. 2, pp. 478–488, April 1988

FAILURE OF SELF-SIMILARITY FOR LARGE ($M_w > 8\frac{1}{4}$) EARTHQUAKES

BY STEPHEN H. HARTZELL AND THOMAS H. HEATON

ABSTRACT

We compare teleseismic *P*-wave records for earthquakes in the magnitude range from 6.0 to 9.5 with synthetics for a self-similar, ω^2 source model and conclude that the energy radiated by very large earthquakes ($M_w > 8\frac{1}{4}$) is not self-similar to that radiated from smaller earthquakes ($M_w < 8\frac{1}{4}$). Furthermore, in the period band from 2 sec to several tens of seconds, we conclude that large subduction earthquakes have an average spectral decay rate of $\omega^{-1.5}$. This spectral decay rate is consistent with a previously noted tendency of the ω^2 model to overestimate M_S for large earthquakes.

INTRODUCTION

The ω^2 spectral model of Aki (1967) and Brune (1970, 1971) is widely used for the general quantification of earthquake sources. The shape of the Brune source spectrum U, regardless of the size of the earthquake, is given by $U(\omega) = A_0\omega_c^2/(\omega_c^2 + \omega^2)$, where ω_c is the spectral corner frequency, and the low-frequency ($\omega < \omega_c$) level A_0 is proportional to the seismic moment M_0. If the average stress drop is independent of M_0, then self-similarity exists among earthquakes (Aki, 1967). Under this condition, the source spectrum of a larger earthquake can be obtained from the spectrum of a smaller one by a simple shift in scales. The corner frequency is then proportional to $M_0^{-1/3}$, and the high-frequency ($\omega > \omega_c$) spectral level is proportional to $M_0^{1/3}$. The ω^2 constant-stress drop model is very appealing, since it reduces the description of the source spectrum to one parameter, M_0, and it has been surprisingly successful in describing the median of a great many seismic observations.

Hanks (1977) compiled estimates of moment and corner frequency based on the ω^2 model for 390 earthquakes, mostly in southern California. He concluded that stress drop is approximately constant, with variations from 1 to 100 bars, in the magnitude range $1.5 \leqq M_w \leqq 7.5$, where $M_w = (\log M_0 - 16.1)/1.5$. The self-similar, ω^2 spectral model has also been used to explain various measures of high-frequency ground motion for earthquakes up to $M_w = 7.7$. Hanks (1979) used Parseval's theorem and Brune's (1970, 1971) spectral scaling to obtain an expression for the rms acceleration observed in the near-source region. Hanks and McGuire (1981) found that a stress drop of 100 bars (to within a factor of 2) could be used to explain average values of rms and peak acceleration for 16 earthquakes in California. The same source spectrum model was used by Boore (1983) to simulate time-domain records. The simulated values of peak acceleration, peak velocity, and response spectra compared favorably with the regression analysis of several hundred strong-motion records by Joyner and Boore (1981, 1982).

In this paper, we present observations of teleseismic P waves from large subduction earthquakes that show systematic deviations from two aspects of the ω^2, self-similar model. These observations suggest that at periods between 2 sec and several tens of seconds: (1) teleseismic P-wave spectral amplitudes fall off at an average rate of $\omega^{-1.5}$, and (2) high-frequency spectral amplitudes do not increase as $M_0^{1/3}$ for earthquakes larger than $M_w\ 8\frac{1}{4}$. The results of earlier studies have already suggested

that this is the case. Boore (1986) examined several source spectrum models, primarily comparing the ω^2 model with the Gusev (1983) model. As previously noted, the ω^2 model does a good job of predicting a wide range of time-domain amplitude measurements. However, it significantly overestimates 20-sec surface wave amplitudes for larger earthquakes ($M_w > 7$). The Gusev source spectrum is constructed to correctly fit the amplitudes of these surface waves and has a region of ω^{-1} spectral decay after an initial ω^{-2} fall-off. Hartzell and Heaton (1985) analyzed Pasadena broadband vertical P-wave records from 63 of the largest, shallow subduction zone earthquakes. They found a wide range of spectral fall-offs from $\omega^{-1.0}$ to $\omega^{-2.25}$ for individual earthquakes with an average spectral fall-off rate of $\omega^{-1.5}$ for periods between 2 sec and several tens of seconds. These calculations were done assuming a constant $t^* = 1.0$ sec. Hartzell and Heaton (1985) also state that if a t^* of 0.5 sec was assumed, then a spectral fall-off of ω^{-2} would be obtained. However, in subsequent calculations, we have found that a t^* of 0.2 sec would be required to change the spectral fall-off from $\omega^{-1.5}$ to $\omega^{-2.0}$, and the assumption of a t^* of 0.5 sec would result in an average spectral fall-off of $\omega^{-1.8}$.

Hartzell and Heaton (1985) also found that, for periods between 2 sec and several tens of seconds, spectral amplitudes of earthquakes larger than M_w $8\frac{1}{4}$ increase with moment at a smaller rate than the $M_0^{1/3}$ predicted by the self-similar ω^2 model. Houston and Kanamori (1986) pointed out that the absolute level of the Hartzell and Heaton (1985) spectra also fall below the level predicted by the ω^2 model. To further pursue these discrepancies, we use a simulation procedure similar to Boore's (1983) to compare peak time-domain amplitudes predicted by the self-similar, ω^2 model with actual records of earthquakes with $6.0 < M_w \leqq 9.5$.

Method

A simulation procedure is used to generate time-domain records which have self-similar, ω^2 source spectra. The method is similar to the procedure used by Boore (1983) to simulate time-domain records for the ω^2 source model for earthquakes with M_w up to 7.7 and by Boore (1986) to compare various spectral models with $\hat{m}_b$ data for earthquakes with M_w up to 9.5. We construct a teleseismic source-time function (Hartzell and Heaton, 1985) that has the desired spectral shape. This source-time function is used to calculate teleseismic synthetic seismograms for specific great earthquakes, complete with the effects of radiation pattern and anelastic attenuation. To assess the validity of the spectral model, the synthetic records are compared with data records from the Pasadena broadband Benioff 1-90 seismometer and several short-period Benioff seismometers located in southern California.

The source-time function is constructed as follows. A pseudo-random number generator that returns values between 0 and 1 is used to fill an array of sample

TABLE 1
Velocity Structure

	α (km/sec)	β (km/sec)	ρ (gm/cm^3)	h (km)
1	5.00	2.88	2.40	8.0
2	5.80	3.34	2.50	9.0
3	7.00	4.04	2.75	16.0
4	8.00	4.62	2.90	—

points having duration $T_c = 1/f_c$, where $f_c = \omega_c/2\pi = 4.9 \times 10^6\ \beta(\Delta\sigma/M_0)^{1/3}$, β is the shear-wave velocity in the source region in kilometers/second, $\Delta\sigma$ is the stress drop in bars, f_c is in Hertz, and M_0 is in dyne-cm (Brune, 1970, 1971). Values of 4.0 km/sec and 15 bars are used for β and $\Delta\sigma$, respectively. (Although 30 bars is the worldwide average stress-drop value, 15 bars is more appropriate for the subduction zone earthquakes considered in this study.) Next, a Gaussian weighting function is used to shape the source-time function in the time domain, followed by transformation to the frequency domain. The amplitude spectrum is then constrained to be the ω^2 spectrum without altering the phase spectrum. The final source-time function is obtained by transforming back to the time domain. Anelastic attenuation is entered with a standard t^* operator equal to 0.7 sec (Futterman, 1962; Carpenter, 1966). The four-layer source-velocity structure given in Table 1 is used in the calculation of the synthetic seismograms. However, a half-space would yield similar results. The source depth is fixed at 30 km with velocities in the source region of α = 7.0 km/sec and β = 4.0 km/sec. Since observed strong ground motions have faster spectral decay rates than ω^{-2} at very high frequencies (Hanks, 1982), Boore (1983) also applies a low-pass filter to the synthetics with a cut-off frequency f_{max} of 15 Hz. No low-pass filter is applied to our synthetics, since f_{max} lies well above the predominant frequency band of the Benioff seismograms used in this study (0.66 and 0.066 Hz for the short-period and broadband Benioff instruments, respectively).

Since the synthetic seismogram depends on the value of the starting seed in the pseudo-random number generator, every synthetic peak amplitude given in this paper is an average of 10 separate determinations with different seeds. The stability of this averaging process was checked by comparing the averages from different sets having 10 runs each. Figure 1 shows some representative self-similar, ω^2 teleseismic source-time functions used to calculate Benioff 1-90 synthetics. A sampling interval of 0.15 sec is used. The short-period Benioff synthetics have a sampling interval of 0.04 sec and time functions similar to those shown in Figure 1. Stability checks verified that average peak record amplitudes did not change when the sampling

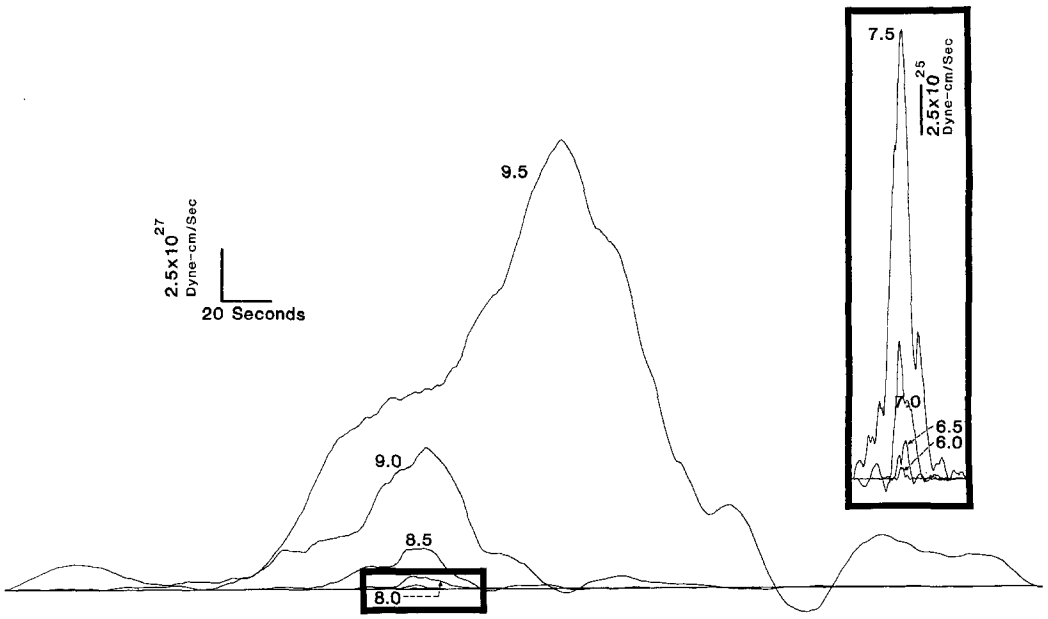

FIG. 1. Constructed teleseismic source-time functions for a self-similar, ω^2 source model.

intervals were varied around these values. The source-time functions in Figure 1 are plotted so that the area under the curve is equal to the moment.

RESULTS

Table 2 lists the observed peak amplitude data for the larger earthquakes considered in this study. The measurements are all in microns for an instrument with unit gain. All broadband 1-90 data are from the Pasadena (PAS) instrument. The 1-90 peak amplitudes do not vary significantly across southern California, and the Pasadena instrument gives representative values (Hartzell and Heaton, 1985). However, there is considerably more variation from site to site in the peak amplitudes of the short-period Benioff records. For this reason, averages of several southern California short-period Benioff stations are used. Table 2 lists the stations used and their individual values. The amplitudes for the 1964 Alaskan earthquake are the largest, and most of the peak motions are not readable. The peak amplitude on the vertical component of the Pasadena 1-90 record is estimated by multiplying the peak values on the horizontal components by 1.6. The short-period Benioff records for the Alaskan earthquake are also difficult to read. Only the Tinemaha record is useable. Tinemaha has the lowest gain in the network (60,000), and as a result, has written on-scale records for most of the largest earthquakes. However, in comparing the peak short-period ground motion amplitudes from the Tinemaha station with those from other stations located across southern California, the Tinemaha records are consistently a factor of 3 to 4 larger. We attribute this discrepancy to local amplification of waves in the sediments beneath Tinemaha. Because of the uncertainties in interpreting the Tinemaha amplitudes, they have not been used in this study, except for the Alaskan earthquake. In the case of the Alaskan earthquake, the Tinemaha short-period amplitude has been corrected downward by a factor of 4.

Observed and synthetic peak amplitudes for the 1-90 and short-period records are summarized in Figures 2 and 3, respectively. Two types of information are plotted: (1) point values for individual earthquakes calculated for the specific mechanism and distance of each earthquake and an average stress drop of 15 bars, and (2) smooth curves of the model amplitudes calculated for a fixed distance (74°) and two values of average stress drop (15 and 30 bars). The theoretical curves are included to show the dependence on stress drop. The smooth curves agree well with curves predicted for the ω^2 model by Heaton *et al.* (1986; equations I.34 through I.40) and the theoretical peak time-domain amplitude scales as M_w for small earthquakes and as $M_w^{1/4}$ for the very largest earthquakes. The smooth curves in Figures 2 and 3 have quite different shapes due to the different responses of the 1-90 and short-period Benioff instruments. Additional data points for smaller earthquakes ($6.0 < M_w < 7.0$) from the Tonga-Kermadec, Japan, and Kurile trenches are also plotted. No model amplitudes are given for these smaller events because their mechanisms are unknown. It is clear from Figure 2 that, for earthquakes larger than about M_w $8\frac{1}{4}$, the self-similar, ω^2 model points (circles) diverge from, and lie significantly above, the observed points (triangles). The same trend, although to a lesser extent, is seen in Figure 3 for the short-period Benioff data. The saturation of the data values at about $M_w = 8\frac{1}{4}$ means that for larger earthquakes, the self-similar, ω^2 model overestimates the amplitude of 15- and 1.5-sec energy (predominant periods in the Benioff 1-90 and short-period records). Houston and Kanamori (1986) found that the peak amplitude on short-period WWSSN instruments at periods near 1.7 sec ($\hat{m}_b$) did not saturate, even at large magnitudes. From our data

TABLE 2

PEAK AMPLITUDE DATA

Event	M_w	Moment ($\times 10^{28}$ dyne-cm)	T_c (sec) $\sigma = 15$ bars	Station*	Peak 1-90 Amplitude (μm)	Peak Short-Period Amplitude (μm)
Miyagi-Oki	7.4	0.22	24.0	PAS	5.9	0.087
06/12/78				RVR		0.025
				BAR		0.031
Tokachi-Oki	8.2	2.8	61.0	PAS	16.7	0.140
05/16/68				RVR		0.150
				MWC		0.080
				BAR		0.090
Kuriles	8.5	7.5	86.0	PAS	12.2	
10/13/63				RVR		0.090
				MWC		0.110
				BAR		0.100
Rat Island	8.7	14.0	108.0	PAS	14.1	0.166
02/04/65				RVR		0.150
				MWC		0.220
				BAR		0.175
				PLM		0.150
Kamchatka	9.0	35.0	152.0	PAS	15.3	0.22
11/04/52				RVR		0.08
				MWC		0.13
				CLC		0.13
Aleutians	9.1	56.0	171.0	PAS	15.3	0.13
03/09/57				RVR		0.11
				BAR		0.12
				PLM		0.15
Alaska	9.2	75.0	192.0	PAS	43.0†	
03/28/64				TIN		0.18‡
Chile	9.5	270.0	271.0	PAS	18.9	
05/22/60				RVR		0.14
				BAR		0.10
				PLM		0.07
				CLC		0.16

* BAR = Barrett; CLC = China Lake; MWC = Mt. Wilson; PAS = Pasadena; PLM = Palomar; RVR = Riverside; and TIN = Tinemaha.

† Estimated from horizontal components.

‡ Corrected for sediment amplification.

set, it appears that there is still saturation at short periods, but to a lesser degree than at longer periods (15 to 20 sec). The fact that the ω^2 model overestimates the long-period amplitude data more than it does the short-period amplitude data is also consistent with the $\omega^{-1.5}$ spectral slope reported by Hartzell and Heaton (1985).

As previously mentioned, the ω^2 model amplitudes for individual earthquakes in Figures 2 and 3 are calculated using an average stress drop of 15 bars. This stress drop gives amplitudes which are close to the observed amplitudes for the magnitude range from $7\frac{1}{4}$ to $8\frac{1}{4}$ (see Miyagi-Oki and Tokachi-Oki points). For $M_w > 8\frac{1}{4}$, an average stress drop of about 7.5 bars is needed to obtain the correct short-period Benioff amplitudes, and an even lower average stress drop of about 3.7 bars is needed to match the amplitudes of the 1-90 data. In other words, the largest earthquakes ($M_w > 8\frac{1}{4}$) are not self-similar to smaller earthquakes. Frequency-

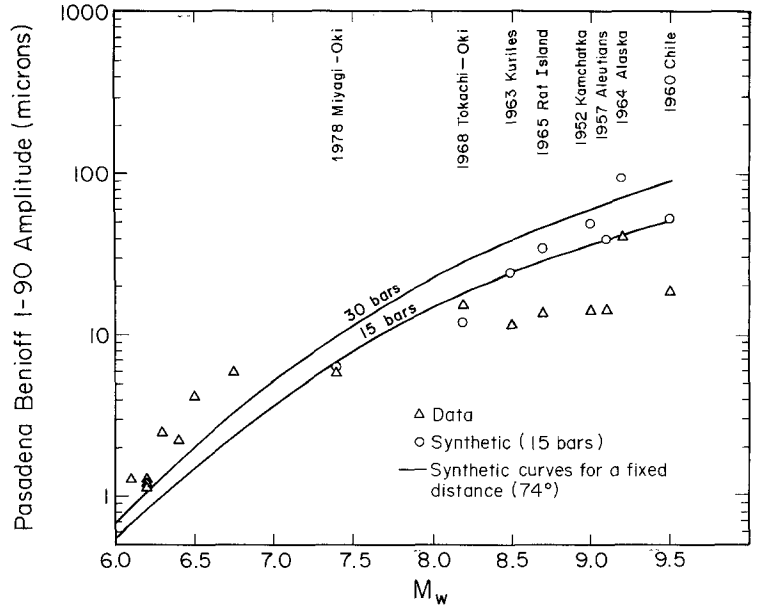

FIG. 2. Peak vertical amplitudes on the Pasadena Benioff 1-90 records compared with self-similar, ω^2 source model synthetics. The synthetic amplitudes (circles) are calculated for the specific mechanism and distance of each earthquake and an average stress drop of 15 bars. The smooth curves are model amplitudes for a fixed distance (74°) and two values of average stress drop (15 and 30 bars). All amplitudes are for an instrument with unit gain.

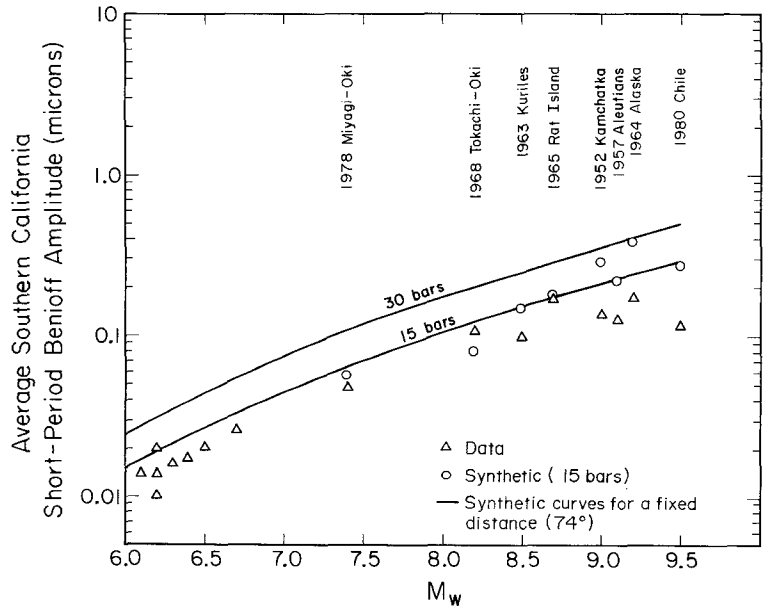

FIG. 3. Average peak vertical amplitudes based on southern California short-period Benioff records compared with self-similar, ω^2 source model synthetics. The synthetic amplitudes (circles) are calculated for the specific mechanism and distance of each earthquake and an average stress drop of 15 bars. The smooth curves are model amplitudes for a fixed distance (74°) and two values of average stress drop (15 and 30 bars). All amplitudes are for an instrument with unit gain.

dependent models of attenuation have a decrease in t^* with frequency beginning in the frequency band 0.1 to 1.0 Hz (Der and Lees, 1985). If such a model were used in this study (instead of a constant t^* of 0.7 sec), there would be negligible change to the results in Figure 2, because the 1-90 amplitudes are determined in the period

range that is relatively insensitive to attenuation. Synthetic amplitudes for the short-period Benioff instrument (Figure 3) would tend to increase; at a period of 1.5 sec, amplitudes would be 1.5 and 2.8 times as large, assuming t^*'s of 0.5 and 0.2 sec, respectively.

Boore (1986) simulated peak time-domain amplitudes for the ω^2 model as modified by Joyner (1984) to allow for two spectral corner frequencies. He compared these amplitudes with values of $\hat{m}_b$ (Houston and Kanamori, 1986) for earthquakes with M_w up to 9.5, and favored a stress drop of 50 bars for a variable attenuation model with $t^* = 0.8$ sec at a period of 1.4 sec. We have repeated his calculations, but favor a lower stress drop. However, the important observation is not the average stress drop level or the value of t^*, since uncertainties in these parameters allow for amplitudes which range over much more than the scatter in the data. Rather, the important observation is that peak amplitudes tend to saturate for $M_w > 8\frac{1}{4}$ compared to the ω^2 self-similar model.

Discussion and Conclusions

The results shown in Figures 2 and 3 are consistent with the observation that the ω^2 model overestimates the amplitude of 20-sec surface waves and the value of M_S (Boore, 1986). The findings of this study are also consistent with the Benioff 1-90 spectra computed by Hartzell and Heaton (1985) for earthquakes with $M_w > 7.0$. Their results are shown in Figure 4. The average high-frequency spectral fall-off is closer to $\omega^{-1.5}$ than $\omega^{-2.0}$. Also, the high-frequency levels for larger magnitude earthquakes ($M_w > 8\frac{1}{4}$) do not increase at the rate of $M_0^{1/3}$, as predicted by the ω^2 model. Instead, the spectral curves begin to coalesce, indicating the same saturation seen in Figures 2 and 3. Therefore, there is compelling evidence that the self-similar, ω^2 model is inconsistent with teleseismic P waves from large subduction earthquakes.

The suggestion that the largest earthquakes ($M_w > 8\frac{1}{4}$) are not self-similar to smaller ones should not be surprising. For subduction earthquakes of less than M_w $8\frac{1}{4}$, rupture length is comparable to rupture width. However, the rupture lengths of

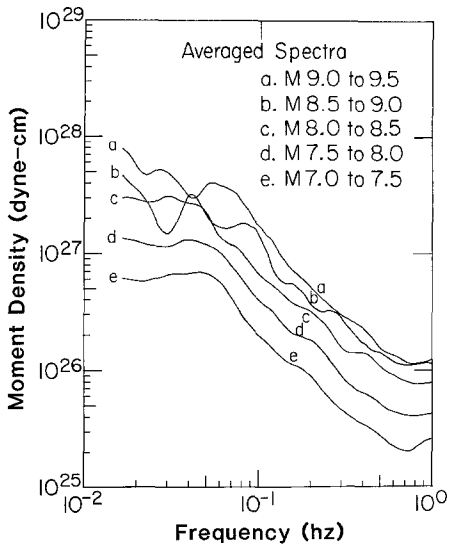

FIG. 4. Benioff 1-90 spectra for large shallow subduction zone earthquakes. Each spectrum is an average of several within the specified magnitude window. The spectra are most accurate between 2 and 50 sec. (From Hartzell and Heaton, 1985.)

the largest earthquakes are many hundreds of kilometers. What is the nature of down-dip rupture when the rupture length is very large? Consider the idealized model shown in Figure 5 in which we assume that the fault rheology varies down-dip. The fact that the seismic moment grows as $S^{3/2}$ (S is rupture area) for even the largest earthquakes (Kanamori and Anderson, 1975; Kanamori and McNally, 1982) is consistent with the hypothesis of large rupture widths (at least several hundred kilometers) for the vary largest earthquakes. If this is the case, then the rupture surfaces of the largest earthquakes ($M_w > 8\frac{1}{4}$) extend into the uppermost mantle. Significant rheological differences would then exist from the top to the bottom of the fault. Under these conditions, the lower portion of the fault may not radiate as much high-frequency energy as the brittle near-surface portion of the fault. However, the deep sections of the fault could still be regions of large moment release. The 1960 Chilean earthquake ($M_w = 9.5$) may be an example of such a rupture process. Kanamori and Cipar (1974) noted that the Pasadena strain record for the Chilean earthquake has a long-period precursor, which when added to the main shock, gives a total moment of 6×10^{30} dyne-cm. This large moment is in apparent contradiction with the measured near-coastal deformation (Plafker and Savage, 1970; Plafker, 1972), the amount of short-period radiation ($T < 20$ sec) (Heaton and Hartzell, 1988), and the measured $\hat{m}_b$ (Houston and Kanamori, 1986). However, all of these observations might be explained by a model in which there is significant moment release in the uppermost mantle, which is removed from the coastal region and is accompanied by little short-period radiation because of the nonbrittle rheology of the mantle.

We show simplified models of fault rupture in Figures 6 and 7. For convenience, we assume that the self-similar, ω^2 model describes seismic radiation from earthquakes having a width less than that of the locked zone (Figure 6). U and E are the spectral amplitude and energy above the corner frequency. In this case, high-frequency radiated energy scales as $M_0^{2/3}$. We hypothesize two alternate physical interpretations for this scaling: (1) high-frequency energy is radiated only from the crack tip and is thus proportional to the rupture area S (using $M_0 \sim S^{3/2}$) or (2) high-frequency energy is radiated throughout the dislocation rise time and is proportional to $(SD)^{2/3}$ (using $M_0 \sim SD$), where D is the average dislocation. These alternative models provide indistinguishable Fourier amplitude spectra assuming the self-similar, ω^2 model (however, these alternative models would be distinguish-

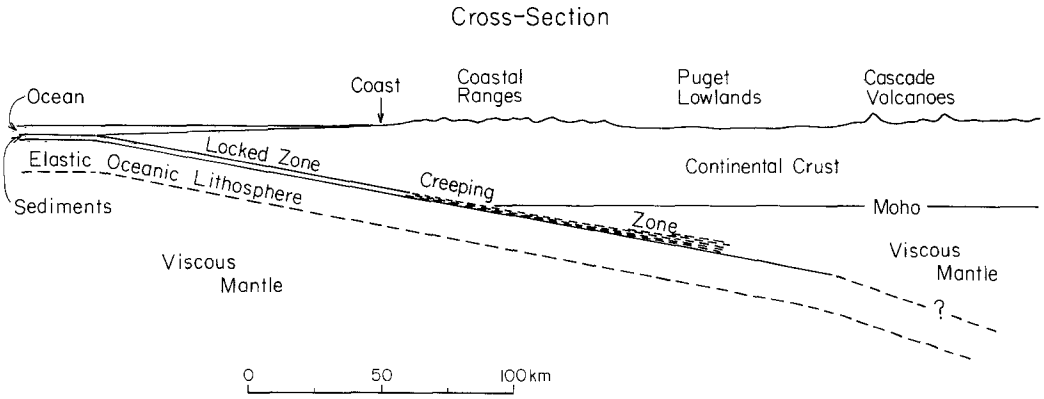

FIG. 5. Schematic model of a subduction zone (Cascadia subduction zone) showing proposed variation of fault properties with depth. In a very large earthquake ($M_w > 8\frac{1}{4}$), we hypothesize that rupture extends into the creeping zone, but that high-frequency energy is only radiated from the shallow, locked section of the fault.

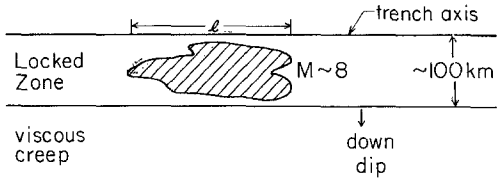

Assume : "Brune Scaling"
constant stress drop
$S \equiv$ rupture area
$\omega_c \equiv$ corner frequency
$D \equiv$ dislocation

$$M_0 \sim \ell^3 \sim S^{3/2}$$

$$U(\omega > \omega_c) \sim M_0^{1/3} \omega^{-2} \sim \ell \omega^{-2}$$

$$E(\omega > \omega_c) \sim \omega^2 U^2(\omega > \omega_c) \sim M_0^{2/3} \omega^{-2}$$

Alternative 1 : $E(\omega > \omega_c) \sim S\omega^{-2}$

Alternative 2 : $E(\omega > \omega_c) \sim S^{2/3} D^{2/3} \omega^{-2}$

FIG. 6. Schematic of self-similar, ω^2 scaling law in which high-frequency energy is radiated everywhere within the rupture zone. Two indistinguishable hypotheses are proposed for this scaling law. In the first, radiated high-frequency energy E is proportional to the rupture area, implying that high-frequency energy is radiated only by the crack tip. In the second, high-frequency energy is radiated throughout the dislocation rise time and high-frequency radiated energy is proportional to $(SD)^{2/3}$.

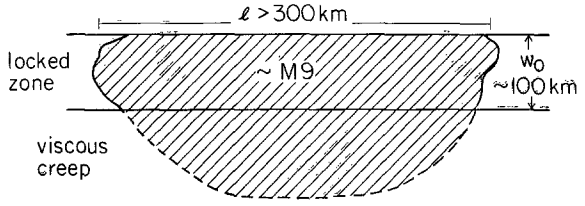

$$M_0 \sim \ell^3 \sim S^{3/2}$$

Assume that high-frequency energy is only radiated from the locked zone.

Alternative 1 : $E(\omega > \omega_c) \sim (\ell w_0)\, \omega^{-2}$

$$U(\omega > \omega_0) \sim \sqrt{\ell w_0}\ \omega^{-2} \sim M_0^{1/6} w_0^{1/2} \omega^{-2}$$

Alternative 2 : $E(\omega > \omega_c) \sim (\ell w_0 D)^{2/3} \omega^{-2} \sim (\ell^2 w_0)^{2/3} \omega^{-2}$

$$U(\omega > \omega_0) \sim \ell^{2/3} w_0^{1/3} \omega^{-2} \sim M_0^{2/9} w_0^{1/3} \omega^{-2}$$

FIG. 7. Schematic of non-self-similar model in which high-frequency energy is only radiated from the locked section of the fault. Slower slip is assumed to occur coseismically in the viscous creeping section of the fault. The two hypotheses of Figure 6 are used to estimate high-frequency spectral amplitudes U as a function of moment.

able in the time domain). In Figure 7, we show a simple model of a very large earthquake in which the rupture extends into a zone of viscous creep. As was the case for smaller earthquakes, we assume that moment continues to grow as $S^{3/2}$. We also assume that high-frequency energy is only radiated from the locked part of the fault. If we assume that radiated high-frequency energy is proportional to the

area of the rupture in the locked zone (hypothesis 1), then we would conclude that high-frequency spectral amplitudes should grow as $M_0^{1/6}$. If we assume that the high-frequency energy is proportional to $(lw_0D)^{2/3}$ (hypothesis 2), where lw_0 is the area of rupture in the locked zone, then high-frequency spectral amplitudes grow as $M_0^{2/9}$. These simple models are examples of non-self-similar scaling laws. A similar scaling law with a slightly different approach has also been introduced by Joyner (1984).

We have also presented evidence that suggests an average spectral decay rate of about $\omega^{-1.5}$ for teleseismic P waves between periods of 2 sec to several tens of seconds for large subduction earthquakes. This spectral decay rate may help to explain the observations of Gusev (1983) who noted that the ω^2 model overestimates 20-sec surface-wave magnitudes M_S. It is beyond the scope of this report to demonstrate a physical model for this phenomenon. However, we believe that this spectral decay is determined by the statistical properties of the rupture process (e.g., roughness). Haskell (1966) and Andrews (1981) give examples of spectral models that are determined by the statistical description of the rupture process. Heaton *et al.* (1986) also discuss spectral models having fractional spectral decay rates.

ACKNOWLEDGMENTS

The authors benefited from discussions with Hiroo Kanamori and David Boore. We also thank Heidi Houston, David Boore, and Stuart Sipkin for their review of the manuscript.

REFERENCES

Aki, K. (1967). Scaling law of seismic spectrum, *J. Geophys. Res.* **72,** 1217–1231.

Andrews, D. (1981). A stochastic fault model. 2. Time-dependent case, *J. Geophys. Res.* **86,** 10821–10834.

Boore, D. (1983). Stochastic simulation of high-frequency ground motions based on seismological models of the radiated spectra, *Bull. Seism. Soc. Am.* **73,** 1865–1894.

Boore, D. (1986). Short-period P- and S-wave radiation from large earthquakes: implications for spectral scaling relations, *Bull. Seism. Soc. Am.* **76,** 43–64.

Brune, J. (1970). Tectonic stress and the spectra of seismic shear waves from earthquakes, *J. Geophys. Res.* **75,** 4997–5009.

Brune, J. (1971). Correction, *J. Geophys. Res.* **76,** 5002.

Carpenter, E. (1966). Absorption of elastic waves—An operator for a constant Q mechanism, Atomic Weapons Research Establishment, Report 0-4366, Her Majesty's Station Office, London, England.

Der, Z. and A. Lees (1985). Methodologies for estimating $t^*(f)$ from short-period body waves and regional variations of $t^*(f)$ in the United States, *Geophys. J. R. Astr. Soc.* **82,** 125–140.

Futterman, W. (1962). Dispersive body waves, *J. Geophys. Res.* **67,** 5279–5291.

Gusev, A. (1983). Descriptive statistical model of earthquake source radiation and its application to an estimation of short-period strong motion, *Geophys. J. R. Astr. Soc.* **74,** 787–808.

Hanks, T. (1977). Earthquake stress drops, ambient tectonic stresses and stresses that drive plate motions, *Pageoph* **115,** 441–458.

Hanks, T. (1979). b values and $\omega^{-\gamma}$ seismic source models: implications for tectonic stress variations along active crustal fault zones and the estimation of high-frequency strong ground motion, *J. Geophys. Res.* **84,** 2235–2242.

Hanks, T. (1982). f_{max}, *Bull. Seism. Soc. Am.* **72,** 1867–1879.

Hanks, T. and R. McGuire (1981). The character of high-frequency strong ground motion, *Bull. Seism. Soc. Am.* **71,** 2071–2095.

Hartzell, S. and T. Heaton (1985). Teleseismic time functions for large shallow subduction zone earthquakes, *Bull. Seism. Soc. Am.* **75,** 965–1004.

Haskell, N. (1966). Total energy and energy spectral density of elastic wave radiation from propagating faults. Part II. A statistical source model, *Bull. Seism. Soc. Am.* **56,** 125–140.

Heaton, T. and S. Hartzell (1988). Estimation of strong ground motions from hypothetical earthquakes on the Cascadia subduction zone, Pacific Northwest, *Pure Appl. Geophys.* (in press).

Heaton, T., F. Tajima, and A. Mori (1986). Estimating ground motions using recorded accelerograms, *Surv. Geophys.* **8,** 25–83.

Houston, H. and H. Kanamori (1986). Source spectra of great earthquakes: teleseismic constraints on rupture process and strong motion, *Bull. Seism. Soc. Am.* **76,** 19–42.

Joyner, W. (1984). A scaling law for the spectra of large earthquakes, *Bull. Seism. Soc. Am.* **74,** 1167–1188.

Joyner, B. and D. Boore (1981). Peak horizontal acceleration and velocity from strong motion records including records from the 1979 Imperial Valley, California, earthquake, *Bull. Seism. Soc. Am.* **71,** 2011–2038.

Joyner, B. and D. Boore (1982). Prediction of earthquake response spectra, *U.S. Geol. Surv., Open-File Rept. 82-977*, 16 pp.

Kanamori, H. and J. Cipar (1974). Focal process of the great Chilean earthquake May 22, 1960, *Phys. Earth Planet. Interiors* **9,** 128–136.

Kanamori, H. and D. Anderson (1975). Theoretical basis of some empirical relations in seismology, *Bull. Seism. Soc. Am.* **65,** 1073–1075.

Kanamori, H. and K. McNally (1982). Variable rupture mode of the subduction zone along the Ecuador-Colombia coast, *Bull. Seism. Soc. Am.* **72,** 1241–1253.

Plafker, G. (1972). Alaskan earthquake of 1964 and Chilean earthquake of 1960, implications for arc tectonics, *J. Geophys. Res.* **77,** 901–925.

Plafker, G. and J. Savage (1970). Mechanism of the Chilean earthquakes of May 21 and 22, 1960, *Geol. Soc. Am. Bull.* **81,** 1001–1030.

U.S. GEOLOGICAL SURVEY
SEISMOLOGY BRANCH
CALIFORNIA INSTITUTE OF TECHNOLOGY, 525-21
PASADENA, CALIFORNIA 91125

Manuscript received 19 May 1987